Sea Ice Surface Temperature Product from the Moderate Resolution Imaging Spectroradiometer (MODIS)

Dorothy K. Hall[1], Jeffrey R. Key[2], Kimberly A. Casey[3], George A. Riggs[3],
and
Donald J. Cavalieri[4]

[1]Code 974, NASA/Goddard Space Flight Center, Greenbelt, MD 20771
dorothy.k.hall@nasa.gov
[2]NOAA/NESDIS, 1225 West Dayton St., Madison, WI 53706
[3]Science Systems and Applications, Inc., Lanham, MD 20706
[4]Code 971, NASA/Goddard Space Flight Center, Greenbelt, MD 20771

Popular Summary

One of the primary instruments on both the Earth Observing System (EOS) Terra and Aqua satellites is the Moderate Resolution Imaging Spectroradiometer (MODIS). Using thermal-infrared bands from MODIS and heritage algorithms, we have developed an algorithm that determines the surface temperature of sea ice, known as the ice-surface temperature (IST) under clear skies at 1-km resolution on a daily, global basis. In this paper, we present the MODIS IST algorithm and show two case studies of validation for the algorithm. One case study, which consisted of 255 samples from MODIS scenes over the South Pole, compared air temperature from the South Pole station with MODIS-derived ISTs. Results showed an uncertainty of <1.7°K in the MODIS measurement. A second case study consisted of 25 samples from MODIS scenes that were compared with air temperatures derived primarily from drifting buoys in the Arctic Ocean, and these results showed an uncertainty of <1.6°K in the MODIS measurement. In both cases, the air temperatures were acquired at a height of about 2 m or greater. We show that the uncertainty in the MODIS measurements would be even lower if actual ISTs could be compared with the MODIS-derived ISTs (since the air temperature at a 2-m height above the ground or ice is different from the temperature of the actual surface). Sea ice IST is an important quantity that is necessary for energy-balance modeling. The MODIS IST maps are the highest-resolution global, daily IST maps available.

Sea Ice Surface Temperature Product from the Moderate Resolution Imaging Spectroradiometer (MODIS)

Dorothy K. Hall[1], *Senior Member, IEEE*, Jeffrey R. Key[2], Kimberly A. Casey[3], George A. Riggs[3], and Donald J. Cavalieri[4]

[1]Code 974, NASA/Goddard Space Flight Center, Greenbelt, MD 20771
dorothy.k.hall@nasa.gov
[2]NOAA/NESDIS, 1225 West Dayton St., Madison, WI 53706
[3]Science Systems and Applications, Inc., Lanham, MD 20706
[4]Code 971, NASA/Goddard Space Flight Center, Greenbelt, MD 20771

Abstract

Global sea ice products are produced from the Earth Observing System (EOS) Moderate Resolution Imaging Spectroradiometer (MODIS) on board both the Terra and Aqua satellites. Daily sea ice extent and ice-surface temperature (IST) products are available at 1- and 4-km resolution. Validation activities have been undertaken to assess the accuracy of the MODIS IST product at the South Pole station in Antarctica and in the Arctic Ocean using near-surface air-temperature data from a meteorological station and drifting buoys. Results from the study areas show that under clear skies, the MODIS ISTs are very close to those of the near-surface air temperatures with a bias of -1.1 and -1.2°K, and an uncertainty of 1.6 and 1.7°K, respectively. It is shown that the uncertainties would be reduced if the actual temperature of the ice surface were reported instead of the near-surface air temperature. It is not possible to get an accurate IST from MODIS in the presence of even very thin clouds or fog, however using both the Advanced Microwave Scanning Radiometer-EOS (AMSR-E) and the MODIS on the Aqua satellite, it may be possible to develop a relationship between MODIS-derived IST and ice temperature derived from the AMSR-E. Since the AMSR-E measurements are generally unaffected by cloud cover, they may be used to complement the MODIS IST measurements.

Introduction

The presence of sea ice influences the temperature and circulation patterns of both the atmosphere and the oceans. Sea ice reduces the amount of solar radiation absorbed at the ocean surface and, with the overlying snow cover, serves as an insulator, restricting exchanges of heat, momentum and chemical constituents between the atmosphere and the ocean. Its large area coverage, 5-8% of the ocean surface, makes the sea ice cover a key parameter in the Earth's energy balance.

The importance of obtaining long-term, climate-data records of sea ice in the form of high-resolution, validated global sea ice maps, is highlighted by recent studies showing decade-scale changes in the global sea ice extent. Several authors have shown that the extent of sea ice in the Arctic has decreased since 1979 by ~3% per decade [1]-[3] and in

addition, the perennial sea ice cover in the Arctic declined at ~9% per decade from 1978 to 2000 [4]. In the Southern Ocean the extent of sea ice increased ~1% per decade from 1979-1998 [5]. Most of these studies have used space-borne coarse-resolution (~25 km) passive-microwave instruments to monitor the sea ice.

Two classes of sensors, microwave and multispectral radiometers, are typically used for global mapping of sea ice extent, concentration, type and temperature. The ability of microwave instruments, both passive and active, to collect data through cloud cover and polar darkness makes them well suited to global monitoring of sea ice extent and dynamics. Passive-microwave data can also provide a measure of ice temperature [6]-[9] though the location within the snow/ice that the temperature represents varies with ice type. However, microwave instruments cannot collect data on sea ice albedo, needed for analysis of energy exchange between the ocean and atmosphere, and they have a relatively coarse spatial resolution which limits their utility for detailed studies of sea ice dynamics. In contrast, visible and/or near-infrared sensors can provide detail on the ice extent and concentration during clear-sky conditions as well as snow/ice albedo and ice-surface temperature (IST). The Moderate Resolution Imaging Spectroradiometer (MODIS), flown on both the Terra and Aqua satellites (launched in December 1999 and May 2002, respectively), is useful for determination of sea ice extent, IST, albedo, movement, type, and concentration at resolutions of 250 m - 1 km.

Daily extent and IST maps are produced using MODIS data at 1-km resolution. In this paper, we describe the algorithm used to create the MODIS IST maps, and provide validation information for this product.

Background

Global year-round records of ice-covered Arctic and Antarctic seas were acquired from several satellite passive-microwave radiometers beginning with the Nimbus-5 Electrically Scanning Multichannel Microwave Radiometer (1972-1977), followed by the Nimbus-7 Scanning Multichannel Microwave Radiometer (1978-1987), and then by the series of Defense Meteorological Satellite Program Special Sensor Microwave/ Imagers (1987-present). The acquisition of microwave radiances from these sensors has allowed the production of hemispheric sea ice concentration maps and global time series of sea ice extent and area [1], [7], [10] & [11]. Sea ice maps have also been available from the National Oceanic and Atmospheric Administration (NOAA) National Ice Center (NIC) since 1972 [12] and are currently available from MODIS (from February 24, 2000, to the present).

Measurement of sea-ice IST is possible with optical sensors such as the Advanced Very High Resolution Radiometer (AVHRR), Landsat Thematic Mapper (TM) and Enhanced Thematic Mapper Plus (ETM+) [13]-[16] and MODIS. Comparisons of AVHRR-derived ice surface temperature with measurements during the Surface Heat Budget of the Arctic (SHEBA) experiment [17] and other field experiments show that the clear-sky IST can be

estimated with an accuracy (root-mean square error) of 0.5 - 1.5°K, depending on the season [18], [19] & [15].

For the retrieval of clear-sky IST, a split-window technique is used, where "split-window" refers to brightness temperature differences in the 11-12 μm atmospheric window. This technique allows for the correction of atmospheric effects, primarily water vapor. First employed to determine sea-surface temperature (SST) [20], the technique was subsequently used to determine IST in the Arctic with the AVHRR on NOAA polar-orbiting satellites [14]. This work was later refined and expanded to include ice surfaces in both polar regions and a broader range of atmospheric conditions. Several other investigators have employed variations of the split-window method for estimation of IST in the polar regions using the AVHRR and other instruments (e.g., [13], [21] & [22]).

MODIS is an imaging spectroradiometer that provides imagery of the Earth's surface and clouds in 36 discrete, narrow spectral bands from approximately 0.4 to 14.0 μm [23]. Global vegetation and land cover, global land-surface change, vegetation properties, surface albedo, land and ice surface temperature and snow and ice cover [24] products from MODIS are available on a daily or regular basis [25]. The spatial resolution of the MODIS instrument varies with spectral band and ranges from 250 m to 1 km at nadir.

MODIS sea ice algorithms

Algorithms for deriving the sea ice map products from MODIS are similar for both the Terra and the Aqua MODIS instruments, and are used to generate maps of sea ice extent as determined by reflectance and IST [26] & [27]. The products are produced globally at both 1-km and ~4-km spatial resolution. During daylight hours, two types of sea ice map products are produced; one is derived from reflectances and the other from IST while at nighttime, only the IST is produced (Table 1). MODIS sea ice products are generated automatically using MODIS sensor radiance data [28], a geolocation product [29], and the MODIS cloud mask product [30], [25] & [26]. In addition to sea ice extent and IST, quality assurance, latitude and longitude, and other information is also included with the data products.

Fig. 1 shows the swath coverage acquired in a region of the Arctic Ocean north of Alaska from Level 1B (L1B) data (left image) and the IST map product (right image). L1B is a swath (scene or granule) of MODIS data geolocated to latitude and longitude centers of 1-km resolution pixels and is available in each of the 36 bands. The MODIS L1B image (left) is shown as a composite of MODIS bands 1 (0.62-0.67 μm), 4(0.545-0.565 μm) and 3 (0.459-0.479 μm). The MODIS IST map (right) also shows ice extent because any pixel that has a temperature of less than 271.5°K is considered to be ice, and any pixel with a temperature of 271.5°K or greater is considered to be open water. Because sea ice is saline, it freezes at a temperature that is less than 273° K; we use 271.5° K as the cutoff temperature between water and ice, although a user can select his/her own cutoff temperature based on the IST to develop a sea ice extent map using the IST.

MODIS sea ice data products are produced as a sequence of products, beginning with a swath (scene) at a nominal pixel spatial resolution of 1 km and a nominal swath coverage of 2330 km (cross track) by 2030 km (along track) (about five minutes of satellite travel), and ends with a global-daily map product (Table 1). Automated selection of the most favorable observation from all the swaths acquired during a day generates a daily gridded sea ice product. A daily global product of sea ice extent and IST at ~4-km resolution in the Equal-Area Scalable Earth Grid (EASEGrid) projection [31] http://nsidc.org/data/ease/ has been developed and is being tested (Fig. 2). Production of this product is expected in the fall of 2003.

There are several different data-product levels starting with Level 2 (L2). An L2 product is a geophysical product that remains in latitude and longitude orientation; it has not been temporally or spatially manipulated. A level-2G (L2G) product is a gridded format of a map projection. At L2G the data products are referred to as tiles, each tile being a piece, e.g., 10° latitude by 10° longitude area, of a map projection. Level-2 data products are gridded into L2G tiles by mapping the L2 pixels into cells of a tile in the map projection grid. The L2G algorithm creates a gridded product necessary for development of the level-3 (L3) products. An L3 product is a geophysical product that has been temporally and or spatially manipulated, and, for sea ice, is gridded into the final product, also an L3 product, a daily global sea ice product for the north and south polar areas in the EASE-Grid projection at ~4-km resolution (Fig. 2).

Both the Terra and Aqua MODIS products may be ordered through the National Snow and Ice Data Center (NSIDC) Distributed Active Archive Center (DAAC) Earth Observing System (EOS) Data Gateway (EDG) at http://nsidc.org/~imswww/pub/imswelcome/index.html [32]. MOD29 is the Earth Science Data Type (ESDT) of the MODIS sea ice products for Terra, and MYD29 is the ESDT for Aqua. "Collection 4" or Version 4 represents the most advanced algorithm, and the products in Collection 4 are improved relative to Collection 3 and earlier collections although at the time of this writing, Collection 4 reprocessing is ongoing but incomplete. When Collection 5 begins in early 2004, all the data will be reprocessed beginning February 24, 2000, to the present into a consistent data set.

The content of the sea ice data products differs between day (MOD29P1D or MYD29P1D) and night (MOD29P1N or MYD29P1N) because MODIS visible data are not acquired when the sensor is in night mode. The day product (MOD29P1D or MYD29P1D) contains both day and nighttime sea ice extent by reflectance and extent by IST while the night product (MOD29P1N or MYD29P1N) contains only IST data processed from MODIS thermal data acquired during the night mode operation of the sensor [26]. These designations should be used when ordering MODIS data from NSIDC.

Sea ice surface temperature. The IST algorithm is the same for both the Terra and Aqua MODIS. For IST, the split-window technique is implemented as a simple regression model of the form

$$T_s = a + bT_{11} + c(T_{11} - T_{12}) + d[(T_{11} - T_{12})(\sec\theta - 1) \qquad [1]$$

where T_s is the surface temperature, T_{11} and T_{12} are the satellite measured brightness temperatures in the 11 and 12 μm channels (MODIS channels 31 and 32), θ is the sensor scan angle, and *a, b, c,* and *d* are regression coefficients. The split-window temperature difference is proportional to the atmospheric water vapor amount, and the scan angle provides information on the path length.

To determine the empirical relationship in eq. [1], radiosonde data from drifting ice and land-based stations were used with a radiative transfer model, LOWTRAN [33], to simulate the sensor brightness temperatures. The sensor spectral response functions were convolved with the calculated radiances and converted to brightness temperatures for each radiosonde profile. The surface temperatures used in the model calculations were then regressed against the simulated brightness temperatures to determine the coefficients in eq. [1]. Radiosonde data poleward of 65° latitude were taken from three archives: the North Pole archive, the National Center for Atmospheric Research (NCAR) archive, and the Historical Arctic Rawinsonde archive [34]. Profile data for Antarctica are from the Antarctic Radiosonde Data Set [35], a compilation of data from 18 land stations, including 16 coastal stations and two interior stations. More than 1000 profiles were used in the each of the Arctic and Antarctic analyses. The spectral, scan angle-dependent emissivities of snow as specified in [15] were used in the radiative transfer calculations. The regression coefficients in eq. [1] were determined separately for the Arctic and Antarctic and for three temperature ranges.

For the AVHRR, some SST methods also employ the 3.7 μm channel. Of course, the use of this channel would be limited to nighttime analyses because it measures emitted thermal energy as well as reflected solar radiation. However, this channel is often noisy at low temperatures when the amount of emitted energy is small, typical of the polar night. For the AVHRR it was found that the inclusion of the 3.7 μm channel in eq. [1] reduced the regression root-mean-square error by only 0.003 K, which we do not consider a significant improvement in accuracy. Nevertheless, both the 3.7 μm and 3.9 μm MODIS channels (channels 20 and 21) will be investigated further in the future to determine if their use will improve the MODIS-derived IST.

Fig. 3a shows a MODIS IST map of sea ice in the northern Greenland Sea. Note the lower ISTs in this map as compared to those in the Arctic Ocean north of Alaska (Fig. 1). The climatological surface air temperature is colder by more than10°K north of Greenland as compared to the Arctic Ocean just north of Alaska (see data from R. Jenne/NCAR in [11]. In both scenes, the recently-refrozen leads are obvious as evidenced by their higher relative temperatures. Well-developed ice floes are evident in the Greenland Sea (Fig. 3a) because this is an active area and near the ice edge, while the area north of Alaska (Fig. 1) is a much more stable area and thus the ice has not been broken apart into distinct floes.

Note the area of the highest ISTs in Fig. 3a, shown in the various shades of red in the southeastern part of the scene. This corresponds to an area of "warmer ice" or of very

low ice concentration approaching the ice edge. Open water (with an IST exceeding 271.5°K) is also visible there. Though the ice edge cannot be seen on the full swath of the MODIS IST product due to obscuration by cloudcover, it is evident on an 89 GHz vertically-polarized Advanced Microwave Scanning Radiometer-EOS (AMSR-E) image shown in Fig. 3b. The location of the MODIS image (Fig. 3a) is shown in the box east-northeast of Greenland in Fig. 3b. The scale represents microwave brightness temperatures (T_{BS}) from 180 - 300°K. Note that there is a general trend toward lower T_{BS} (Fig. 3b) and lower ISTs (Fig. 3a) toward the northwest in the rectangular study area.

Land and Cloud Masking in the Data Products. Land is masked using the 1-km resolution United States Geological Survey (USGS) global land/water mask [36] stored in the MODIS geolocation product [29]. The land/water mask is used by both the sea ice algorithm and cloud-masking algorithm to determine if a pixel is land or ocean for processing in the algorithms. An issue with this land/water mask is that ice shelves, such as the Ross Ice Shelf of Antarctica, are classified as land and not as part of the ocean because they emanate from the ice sheet. Consequently, ice shelves have not been included in the MODIS sea ice products. Improved coastline data that maps ice shelves as ocean have been developed and will be integrated into a future improved land/water mask. Following its implementation, it will be possible to monitor large icebergs that calve from the ice shelves in Antarctica.

Many situations occur that make it very difficult to identify clouds over sea ice in the daytime or nighttime even with the many visible and infrared MODIS bands. If the MODIS cloud mask reports a "certain cloud" condition for a pixel, then the sea ice product is reported as cloud for that same pixel [30]. If the cloud mask reports that the observation is "probably clear," or "confident clear," then it is interpreted as clear and the sea ice algorithm analyzes the pixel for IST.

The accuracy of the MODIS cloud mask over snow and ice varies, with the highest accuracy generally found for daytime data and the lowest accuracy in darkness. Low illumination and the similar reflectance characteristics of clouds and sea ice at visible wavelengths cause difficulties in cloud masking using MODIS data. Additionally, atmospheric inversions can cause surface temperatures to be colder than the temperature of some clouds, e.g., [37]. Snow/cloud discrimination problems are compounded during the polar night because the MODIS reflective bands are not useful during darkness. The absolute accuracy of the MODIS cloud mask used in the sea ice algorithm is not known. The Aqua MODIS cloud mask algorithm was revised to use band 7 (2.1 μm) in place of band 6 (1.6 μm) because most of the detectors on the Aqua MODIS in band 6 are non-functional. The revised Aqua cloud mask algorithm has been in operation since May 20, 2003, and has affected the masking of clouds over sea ice relative to the cloud mask used with the Terra MODIS products.

A particular problem for mapping clouds over sea ice is the identification of thin clouds and fog. Fog often develops in sea ice covered waters when water vapor forms following the formation of leads and polynyas. While it may be possible to see the sea ice on a

MODIS image, and even map the sea ice through the fog, it is not possible to retrieve an accurate IST through fog, even with the many visible and infrared MODIS bands.

IST Validation

In order to determine the accuracy of the MODIS-derived IST measurements, MODIS-derived skin temperature and the observed surface air (not skin) temperature at South Pole were compared (Fig. 4). Though a land site, the South Pole is a good study site because surface-based cloud measurements are available. The results represent primarily nighttime cases, and are from April through December 2001. Scenes were identified as clear by examining micropulse lidar data at the South Pole station. The closest pixel was used, i.e., no averaging of adjacent pixels was done. There is a bias -1.2°K, and a root-mean-square error (RMSE) or uncertainty of 1.7°K where the satellite-derived skin temperature is, on average, lower than the measured surface air temperature. This difference is almost certainly due to the skin and air temperature differences that are common in the presence of atmospheric temperature inversions. The variability in the two measurements is greatest for low surface temperatures, possibly due to the lower radiometric accuracy of the MODIS infrared channels at such extreme temperatures.

Validation in the Arctic Ocean was also conducted. Data from the National Oceanic and Atmospheric Administration (NOAA) Center for Operational Oceanographic Products and Service (NOAA/NOS CO-OPS) program (http://www.co-ops.nos.noaa.gov/co-ops.html) meteorological station located at the Prudhoe Bay tide station data in Prudhoe Bay, AK (70° 24.0' N, 148° 31.6' W) were studied. The Prudhoe Bay tide station, established in July 1990, is located at the end of a causeway north of Prudhoe Bay. The air temperature measurements are acquired at a height of ~9 m above sea level [38]. The tide station also provides information on tides (water level) and barometric pressure, wind speed, direction and gust, including hourly air and water temperature data.

An average of MODIS pixels nearest to the NOAA tide station at Prudhoe Bay, Alaska, was used to determine the IST at the time of the MODIS overpass. The pixel nearest the Prudhoe Bay tide station was used, along with 2 to 5 immediate surrounding pixels (exclusive of cloud and land pixels). This was matched with the nearest (in time) air temperature provided by the NOAA/NOS CO-OPS program through the website shown above.

Air temperatures from drifting buoys were also used to validate the Terra and Aqua MODIS IST maps. The North Pole Environmental Observatory (NPEO) provides long-term measurements that are needed to track changes in the Arctic environment, including an automated drifting station consisting of clusters of buoys fixed to the drifting sea ice [39]. The buoys, tracked with global-positioning system receivers, measure atmospheric, ice and other geophysical quantities in the Arctic Ocean. Air temperature is acquired at a height of ~1.2 m. The Japan Marine Science and Technology Center (JAMSTEC) Compact Arctic Drifter #1, or J-CAD 1, was the first in a series that began

acquiring measurements in April 2000 in the Arctic Ocean. For validation of the MODIS IST we used data from J-CAD 4 and 5 as well as from the Prudhoe Bay tide station.

Radionov et al. [40] show that in the Arctic Basin during the winter when the cloud cover is continuous, the snow surface temperature did not differ from the air temperature measured at a height of 2 m. However, under cloud-free conditions, the difference between those temperatures reached 6-7°K, the snow temperature being sharply lower compared with the 2-m air temperature due to longwave radiative cooling when the sky was clear. During the Arctic cold period, defined as October through May, the average temperature of the snow (250 measurements per month) was lower by an average of 0.6°K than the 2-m air temperature. During the warm period, defined as June through August, the average temperature of the snow was 0.7°K lower than the 2-m air temperature (125 - 246 measurements per month) [40]. Based on this information, a bias of at least 0.6°K should be considered when comparing air temperature measurements from the Prudhoe Bay Co-op station and the drifting buoys to the MODIS IST retrievals. All of our data (Table 2) were acquired during the "cold period" as defined above. Since the Prudhoe Bay in-situ air temperatures were acquired from a height of ~9 m, one would expect this difference to be even greater.

Table 2 summarizes the Prudhoe Bay tide station and the Arctic drifting buoy results. Fig. 5 shows a comparison of the meteorological station or buoy temperatures and the MODIS-derived ISTs using 25 scenes that were deemed cloud-free at the measurement site. This data set reveals a bias of –1.1°K and a RMSE or uncertainty of 1.6°K, values that are close to those calculated for the South Pole data set (Fig. 4). If we adjust the air temperatures of the co-op station and the drifting buoys in accordance with the Radinov et al. results for the "cold period," 0.6°K, then the adjusted bias is –0.46°K with an uncertainty of 1.3°K. However, because the meteorological station data and buoy data were acquired at a height of 1.2 and 9 m, respectively, and because the IST retrievals are for clear-sky conditions, it is difficult to have confidence in that exact number since the Radinov et al. measurements were made at a height of 2 m.

Limitations

A considerable amount of visual study was required to avoid selecting MODIS pixels that appeared to be cloud contaminated. Only about 14% of the MODIS scenes selected were used. The rest of the scenes were rejected for a variety of reasons. The main reason for rejection of a daytime scene was that clouds were observed in the L1B companion scene near the buoy or tide station. Additionally, when the difference between the MODIS and in-situ IST was large (~3° or greater) and there was a possibility of cloud contamination (e.g., clouds were nearby), or there was no L1B scene available due to darkness, the scene was rejected. As a result, the results in Table 2 are considerably better than would be the case if the scenes were selected randomly from "cloud-free" parts of the MODIS maps as determined from the MODIS cloud mask.

Though the MODIS-derived IST algorithm performs extremely well under totally clear-sky conditions, polar weather is often a factor that influences negatively the quality of the derived IST. It is virtually impossible to determine whether conditions are completely cloud free when deriving IST in an automated way using the MODIS cloud mask algorithm summary result flag of "certain cloud." That summary result is based on several cloud tests applied in the cloud mask algorithm and confidences associated with the tests. In some situations the tests can fail to detect clouds or may detect clouds falsely resulting in an inaccurate result. Improved cloud masking results have been attained in the MODIS snow algorithm when selected cloud tests from the MODIS cloud mask are used to create a cloud mask specific to snow-covered land surfaces. Selective use of individual cloud tests from the MODIS cloud mask product should result in improved cloud masking relevant to the IST algorithm as has been the case for the MODIS snow maps [41].

Discussion and Conclusions

The 1-km MODIS daily IST product represents the only global IST product available at such a fine resolution and may be used for energy-balance modeling. The clear-sky limitation can possibly be obviated using passive-microwave data in conjunction with MODIS data. Passive-microwave-derived ice temperatures are not directly comparable with ISTs because the passive-microwave temperature is an integrated measure of the temperature of the upper layers of the sea ice or/and overlying snow cover and the depth of penetration depends on the emissivity of the snow/ice. However, if a relationship can be determined between MODIS-derived ISTs and passive-microwave-derived ice temperature, then the passive-microwave derived ice temperatures can be used to approximate IST even through clouds. Such a product would provide modelers global IST data daily through cloudcover and darkness though at a coarser resolution than is possible from MODIS if MODIS could be used alone.

With both the AMSR-E and the MODIS on the Aqua satellite, it will be possible to assess the relationship between MODIS-derived IST and ice temperature derived from the AMSR-E. The recent launches of the AMSR sensors on the EOS Aqua and Advanced Earth Observing Satellite II (ADEOS II) spacecraft and the planned Defense Meteorological Satellite Program (DMSP) Special Sensor Microwave Imager/Sounder (SSMIS) and the National Polar-orbiting Operational Environmental Satellite System (NPOESS) missions will extend the sea ice records into the foreseeable future.

The MODIS sea ice products represent a suite of products that is useful for long-term climate-data records. Additional work will need to be done in order to validate the products for a variety of ice types and geographic locations. However the MODIS IST product appears to be of comparable or superior quality as compared to predecessor data sets, such as products derived from the AVHRR, and should compare well with products that will be derived from future sensors for sea ice extent and IST.

The MODIS-derived IST provides an excellent measurement of the actual temperature of the surface of the sea ice under clear skies. Two different validation studies from the South Pole and the Arctic Ocean show excellent agreement, with a bias of -1.1 and -1.2 °K, and an uncertainty of 1.6 and 1.7 °K, respectively.

Acknowledgments

The authors would like to thank Yinghui Liu, Cooperative Institute for Meteorological Satellite Studies,University of Wisconsin, for providing the South Pole IST plot; and the North Pole Environmental Observatory for use of the drifting buoy data; and Nick DiGirolamo and Al Ivanoff of SSAI for providing programming support. The AMSR-E instrument was provided by Japan's National Space Development Agency. The funding for this work was provided by the EOS Project in NASA's Earth Science Enterprise.

References

[1] D. J. Cavalieri, P. Gloersen, C.L. Parkinson, J.C. Comiso and H.J. Zwally, "Observed asymmetry in global sea ice changes," *Science,* vol. 278, pp. 1104-1106, 1997.

[2] K. Y. Vinnikov, A. Robock, R.J. Stouffer, J.E. Walsh, C.L. Parkinson, D.J. Cavalieri, J.F.B. Mitchell, D. Garrett and V.F. Zakharov, "Global warming and Northern Hemisphere sea ice extent," *Science,* vol. 286, pp. 1934-1937, 1999.

[3] C. L. Parkinson and D.J. Cavalieri, "A 21 year record of Arctic sea-ice extents and their regional, seasonal and monthly variability and trends," *Annals of Glaciology,* vol. 34, pp. 441-446, 2002.

[4] J. C. Comiso, "A rapidly declining perennial sea ice cover in the Arctic," *Geophysical Research Letters*, vol. 29(20), 1956, doi:10.1029/2002GL015650, 2002.

[5] H. J. Zwally, J. C. Comiso, C. L. Parkinson, D. J. Cavalieri, and P. Gloersen, "Variability of Antarctic Sea Ice 1979-1998," *Journal of Geophysical Research*, vol. 107 (C5):10.1029/2000JC000733, 2002.

[6] D. J. Cavalieri, P. Gloersen, and W. J. Campbell, "Determination of sea ice parameters with the Nimbus-7 SMMR," *Journal of Geophysical Research*, vol. 89, pp. 5355-5369, 1984.

[7] P. Gloersen, W. J. Campbell, D. J. Cavalieri, J. C. Comiso, C. L. Parkinson, H. J. Zwally, "Arctic and Antarctic Sea Ice, 1978-1987: Satellite Passive Microwave Observations and Analysis," National Aeronautics and Space Administration, Special Publication 511, Washington, D.C., pp.290, 1992.

[8] C. A. Shuman, R.B. Alley, S. Anandakrishnan and C.R. Stearns, "An empirical technique for estimating near-surface air temperature trends in central Greenland from SSM/I brightness temperatures," *Remote Sensing of Environment,* vol. 51, pp. 245-252, 1995.

[9] J. C. Comiso, D.J. Cavalieri and T. Markus, "Sea ice concentration, ice temperature, and snow depth using AMSR-E data," *IEEE Transactions on Geoscience and Remote Sensing,* vol. 41(2), pp. 243-252, 2003.

[10] H. J. Zwally, J.C. Comiso, C.L. Parkinson, W.J. Campbell, F.D. Carsey and P. Gloersen, "Antarctic Sea Ice, 1973-1976: Satellite Passive-Microwave Observations," NASA SP-459, 206 p. GPO, Washington, D.C., 1983.

[11] C. L. Parkinson, J.C. Comiso, H.J. Zwally, D.L. Cavalieri, P. Gloersen and W.J. Campbell, "Arctic Sea Ice, 1973-1976: Satellite Passive-Microwave Observations," NASA SP-487, GPO, Washington, D.C., 1987.

[12] K. R. Dedrick, K. Partington, M. Van Woert, C.A. Bertoia and D. Benner, "U.S. National/Naval Ice Center digital sea ice data and climatology," *Canadian Journal of Remote Sensing,* vol. 27(5), pp. 457-475, 2001.

[13] R. W. Lindsay and D.A. Rothrock, "Arctic sea ice surface temperature from AVHRR," *Journal of Climate*, vol. 7(1), pp. 174-183, 1993.

[14] J. Key and M. Haefliger, "Arctic ice surface temperature retrieval from AVHRR thermal channels," *Journal of Geophysical Research*, vol. 97(D5), pp. 5885-5893, 1992.

[15] J. Key, J. Collins, C. Fowler, and R. Stone, "High-latitude surface temperature estimates from thermal satellite data," *Remote Sensing Environment*, vol. 61, pp. 302-309, 1997.

[16] J. C. Comiso, "Satellite-observed variability and trend in sea-ice extent, surface temperature, albedo and clouds in the Arctic," *Annals of Glaciology,* vol. 33, pp. 457-473, 2001.

[17] R. E. Moritz, J.A. Curry, N. Untersteiner, and A.S. Thorndike, "*Prospectus: Surface heat budget of the Arctic Ocean*," NFSF-ARCSS OAII Tech. Rep. 3, 33 pp. Available from the SHEBA Project Office, Polar Science Center, Applied Physics Laboratory, University of Washington, Seattle, WA 98105, 1993.

[18] J. Maslanik, J. Key, C. Fowler, T. Nyguyen, X. Wang, "Spatial and temporal variability of surface and cloud properties from satellite data during FIRE-ACE," *Journal of Geophysical Research*, vol. 106(D14), pp. 15233-15249, 2001.

[19] J. Key, J.A. Maslanik, T. Papakyriakou, M.C. Serreze, and A.J. Schweiger, "On the validation of satellite-derived sea ice surface temperature," *Arctic*, vol. 47(3), pp. 280-287, 1994.

[20] C. P. Prabhakara, G. Dalu and V.G. Kunde, "Estimation of sea surface temperature from remote sensing in the 11 – 13 μm window region," *Journal of Geophysical Research,* 79(33):5039-5044, 1974.

[21] R. Massom and J.C. Comiso, "The classification of Arctic sea ice types and the determination of surface temperature using advanced very high resolution radiometer data," *Journal of Geophysical Research*, vol. 99(C3), pp. 5201-5218, 1994.

[22] Y. Yu, D.A. Rothrock, and R.W. Lindsay, "Accuracy of sea ice temperature derived from the advanced very high resolution radiometer," *Journal of Geophysical Research*, vol. 100, pp. 4525-4532, 1995.

[23] W. L. Barnes, T.S. Pagano and V.V. Salomonson, "Prelaunch characteristics of the Moderate Resolution Imaging Spectroradiometer (MODIS) on EOS-AM1," *IEEE Transactions on Geoscience and Remote Sensing,* vol. 36(4), pp. 1088-1100, 1998.

[24] D. K. Hall, G.A. Riggs, V.V. Salomonson, N.E. DiGirolamo and K.J. Bayr, "MODIS snow-cover products," *Remote Sensing of Environment,* vol. 83, pp. 181-194, 2002.

[25] C. O. Justice and 22 others, "The Moderate Resolution Imaging Spectroradiometer (MODIS): land remote sensing for global change research," *IEEE Transactions on Geoscience and Remote Sensing*, vol. 36(4), pp. 1228-1249, 1998.

[26] G. A. Riggs, D.K. Hall and V.V. Salomonson, "MODIS Sea Ice User's Guide," http://modis-snow-ice.gsfc.nasa.gov/siugkc.html, 2003.

[27] G. A. Riggs, D.K. Hall, and S.A. Ackerman, "Sea Ice Extent and Classification Mapping with the Moderate Resolution Imaging Spectroradiometer Airborne Simulator," *Remote Sensing of Environment*, vol. 68, pp. 152-163, 1999.

[28] B. Guenther, X. Xiong, V.V. Salomonson, W.L. Barnes and J. Young, "On-orbit performance of the Earth Observing System Moderate Resolution Imaging Spectroradiometer; first year of data," *Remote Sensing of Environment,* vol. 83, pp. 16-30.

[29] R. Wolfe, M. Nishihama, A.J. Fleig, J.A. Kuyper, D.P. Roy, J.C. Storey and F.S. Patt, "Achieving sub-pixel geolocation accuracy in support of MODIS land science," *Remote Sensing of Environment,* vol. 83, pp. 31-49, 2002.

[30] S. A. Ackerman, K. I. Strabala, P. W.P. Menzel, R.A. Frey, C.C. Moeller and L.E. Gumley, "Discriminating clear sky from clouds with MODIS," *Journal of Geophysical Research*, vol. 103(D24), pp. 32,141-32,157, 1998.

[31] R. L. Armstrong and M.J. Brodzik, "An earth-gridded SSM/I data set for cryospheric studies and global change monitoring," *Advances in Space Research,* vol 10, pp. 155-163, 1995.

[32] G. R. Scharfen, D.K. Hall, S.J.S. Khalsa, J.D. Wolfe, M.C. Marquis, G.A. Riggs and B. McLean, "Accessing the MODIS snow and ice products at the NSIDC DAAC," *Proceedings of IGARSS'00*, 23-28 July 2000, Honolulu, HI, pp. 2059-2061, 2000.

[33] F. X. Kneizys, E.P. Shettle, L.W. Abreu, J.H. Chetwynd, G.P. Anderson, W.O. Gallery, J.E.A. Selby, and S.A. Clough, "Users Guide to LOWTRAN 7," AFGL-TR-88-0177, *Environmental Research Papers*, No. 1010, 137 p., 1988.

[34] M. C. Serreze, J.D. Kahl, and R.C. Schnell, "Low-level temperature inversions of the Eurasian Arctic and comparisons with Soviet drifting station data," *Journal of Climate*, vol. 5(6), pp. 615-629, 1992.

[35] W. M. Connolley and J.C. King, "Atmospheric water vapour transport to Antarctica inferred from radiosondes," *Quarterly Journal of the Royal Meteorology Society*, vol. 119, pp. 325-342, 1993.

[36] USGS, "*Landsat 7 image assessment system geometric Algorithm Theoretical Basis Document*," Version 2, J.C. Storey (ed.), USGS EROS Data Center, 1997.

[37] T. J. McIntire and J.J. Simpson, "Arctic sea ice, cloud, water, and lead classification using neural networks and 1.6 μm data," *IEEE Transactions on Geoscience and Remote Sensing,* vol. 40(9), pp. 1956-1972, 2002.

[38] M. J. McCray, written communication, NOAA/National Ocean Service, 2003.

[39] J. H. Morison, K. Aagaard, K.K. Falkner, K. Hatakeyama, R. Moritz, J.E. Overland, D. Perovich, K. Shimada, M. Steele, T. Takizawa and R. Woodgate, "North Pole Environmental Observatory delivers early results," *EOS*, vol. 83(33), pp. 357, 360-361, 2002.

[40] V. F. Radionov, N.N. Bryazgin and E.I. Alexandrov, "The snow cover of the Arcitc Basin," Applied Physics Laboratory, University of Washington, Technical Report APL-UW TR 9701, 1997.

[41] G. A. Riggs and D. K. Hall, "Reduction of Cloud Obscuration in the MODIS Snow Data Product," Presented at the 59th Eastern Snow Conference, 5-7 June 2002, Stowe, VT, http://modis-snow-ice.gsfc.nasa.gov/publications.html, 2002.

List of Figures

Figure 1. Left - True-color MODIS image using bands 1 (0.62-0.67 μm), 4(0.545-0.565 μm) and 3 (0.459-0.479 μm) derived from Terra MODIS Level 1B data, March 6, 2003 (22:45 UTC), in the Arctic Ocean north of Alaska; Right - MODIS ice-surface temperature (IST) map product of the same area at the same date and time. The location of the J-CAD 5 drifting buoy is shown inside the small yellow box at 76.91° N, 162.50° W (upper left). The color scale represents IST in °K.

Figure 2. Prototype of the sea ice-surface temperature (IST) global EASE-Grid composite product of the north polar area (average of May 15-19, 2000), MOD29C2. Color key shows ISTs from 230-271°K. The color scale represents IST in °K.

Figure 3. a) Terra MODIS ice-surface temperature (IST) product (MOD29) acquired on March 12, 2003 (18:45 UTC), in the northern Greenland Sea in the Arctic Ocean. The approximate center point of the image is 81.7° N, 1.0° E. The color scale represents IST in °K. b) Advanced Microwave Scanning Radiometer-EOS (AMSR-E) 89 GHz vertically-polarized image from the Aqua satellite, averaged from several swaths of data acquired on March 12, 2003, at a spatial resolution of ~5 km. The rectangular box east-northeast of Greenland is the area of the MODIS IST image from Fig. 3a. Microwave brightness temperatures (T_Bs) from 180-300°K are shown in the scale.

Figure 4. MODIS IST retrieved temperatures and measured surface temperatures at the South Pole in Antarctica. Results are from a comparison of MODIS-derived skin temperature and the observed surface air (not skin) temperature at South Pole, primarily nighttime cases for the period April-December 2001. Scenes were identified as clear by examining micropulse lidar data at South Pole. The closest pixel was used, i.e., no averaging was done.

Figure 5. MODIS IST retrieved temperatures and measured surface temperatures at three locations in the Arctic Ocean on various dates between January 25, 2002, and May 9, 2003. Most of the measured temperatures were acquired from buoy data (see text for explanation), but a few were acquired from the tide station at Prudhoe Bay, AK (see text for explanation).

List of Tables

Table 1. MODIS sea ice data products.

Table 2. IST validation summary for J-CAD 4 and 5 drifting buoys, and the Prudhoe Bay tide station. "Terra" and "Aqua" refer to images acquired from either the Terra or Aqua MODIS instruments, and 003 and 004 refer to either version 3 or 4 of the MODIS IST algorithm. Buoy or station temperatures are subtracted from the MODIS ISTs to derive the difference.

Table 1. MODIS sea ice data products.

Long Name	Earth Science Data Type (ESDT)	Spatial Resolution
MODIS/Terra Sea Ice Extent 5-Min L2 Swath 1km	MOD29	1-km resolution, swath of MODIS data
MODIS/Terra Sea Ice Extent Daily L3 Global EASE-Grid Day	MOD29P1D	1-km resolution, projected, gridded tile data
MODIS/Terra Sea Ice Extent Daily L3 Global EASE-Grid Night	MOD29P1N	1-km resolution, projected, gridded tile data
MODIS/Terra Sea Ice Extent and Ice Surface Temperature Daily L3 Global 4km EASE-Grid Day *	MOD29E1D	4-km resolution, global, gridded
MODIS/Terra Ice Surface Temperature Daily L3 Global 4km EASE-Grid Night *	MOD29E1N	4-km resolution, global, gridded
MODIS/Terra Sea Ice Extent and Ice Surface Temperature 8-Day L3 Global EASE-Grid Day **	MOD29E2D	4-km resolution, global, gridded
MODIS/Terra Ice Surface Temperature 8-Day L3 Global EASE-Grid Night**	MOD29E2N	4-km resolution, global, gridded
MODIS/Terra Sea Ice Extent and Ice Surface Temperature Monthly L3Global 4km EASE-Grid Day**	MOD29EMD	4-km resolution, global, gridded
MODIS/Terra Ice Surface Temperature Monthly L3Global 4km EASE-Grid Night **	MOD29EMN	4-km resolution, global, gridded
MODIS/Aqua Sea Ice Extent 5-Min L2 Swath 1km	MYD29	1-km resolution, swath of MODIS data
MODIS/Aqua Sea Ice Extent Daily L3 Global EASE-Grid Day**	MYD29P1D	1-km resolution, projected, gridded tile data
MODIS/Aqua Sea Ice Extent Daily L3 Global EASE-Grid Night**	MYD29P1N	1-km resolution, projected, gridded tile data
MODIS/Aqua Sea Ice Extent and Ice Surface Temperature Daily L3 Global 4km EASE-Grid Day*	MYD29E1D	4-km resolution, global, gridded
MODIS/Aqua Ice Surface Temperature Daily L3 Global 4km EASE-Grid Night *	MYD29E1N	4-km resolution, global, gridded
MODIS/Aqua Sea Ice Extent and Ice Surface Temperature 8-Day L3 Global EASE-Grid Day **	MYD29E2D	4-km resolution, global, gridded
MODIS/Aqua Ice Surface Temperature 8-Day L3 Global EASE-Grid Night**	MYD29E2N	4-km resolution, global, gridded
MODIS/Aqua Sea Ice Monthly Global EASE-Grid **	MYD29EMD	4-km resolution, global, gridded

*Future enhancement or product (to be implemented in fall 2003).

**Future enhancement or product (to be implemented in 2004).

Table 2. IST validation summary for J-CAD 4 and 5 drifting buoys, and the Prudhoe Bay tide station. "Terra" and "Aqua" refer to images acquired from either the Terra or Aqua MODIS instruments, and 003 and 004 refer to either version 3 or 4 of the MODIS IST algorithm. Buoy or station temperatures are subtracted from the MODIS ISTs to derive the difference.

J-CAD 4 – JAMSTEC buoy

Date	Time (UTC) – data specification	MODIS IST °K	J-CAD 4 buoy °K	Difference °K
Mar 1 2003	1905 – Terra 004	234.5	235.9	-1.4
Mar 2 2003	1810 – Terra 004	239.1	240.2	-1.1
Mar 3 2003	0250 – Aqua 003	237.1	238.9	-1.8
Mar 3 2003	0745 – Aqua 003	237.8	239.7	-1.9
Mar 3 2003	1100 – Aqua 003	238.3	240.2	-1.9
Mar 9 2003	1500 – Terra 004	243.8	243.9	-0.1
Apr 14 2003	2105 – Terra 004	269.7	268.4	1.3
Apr 15 2003	2010 – Terra 004	270.5	270.9	-0.4

J-CAD 5 – JAMSTEC buoy

Date	Time (UTC) – data specification	MODIS IST °K	J-CAD 5 buoy °K	Difference °K
Mar 6 2003	2245 – Terra 004	254.4	256.7	-2.3
Mar 7 2003	0200 – Terra 004	252.1	254.4	-2.3
Mar 29 2003	0755 – Terra 004	247.4	249.9	-2.5
Apr 16 2003	0250 – Terra 004	251.7	253.9	-2.2
Apr 16 2003	2240 – Terra 004	250.6	250.9	-0.3
May 8 2003	2340 – Terra 004	262.4	262.4	0.0
May 9 2003	0255 – Terra 004	261.5	262.4	-0.9

Prudhoe Bay, AK - NOAA tide station

Date	Time (UTC) – data specification	MODIS IST °K	Prudhoe Bay °K	Difference °K
Jan 25 2002	2230 – Terra 003	235.3	235.3	0.0
Mar 3 2002	2100 – Terra 003	245.0	244.7	0.3
Mar 29 2002	2145 – Terra 003	248.1	248.3	-0.2
Mar 30 2002	2230 – Terra 003	250.1	248.5	1.6
Mar 31 2002	2135 – Terra 003	251.5	251.1	0.4
May 21 2002	2205 – Terra 003	272.9	275.7	-2.8
May 22 2002	2110 – Terra 003	273.3	275.9	-2.6
Nov 20 2002	2210 – Terra 003	249.9	252.5	-2.6
Jan 19 2003	2055 – Terra 004	254.9	256.3	-1.4
Jan 19 2003	2235 – Terra 004	255.8	257.4	-1.6

Figure 1

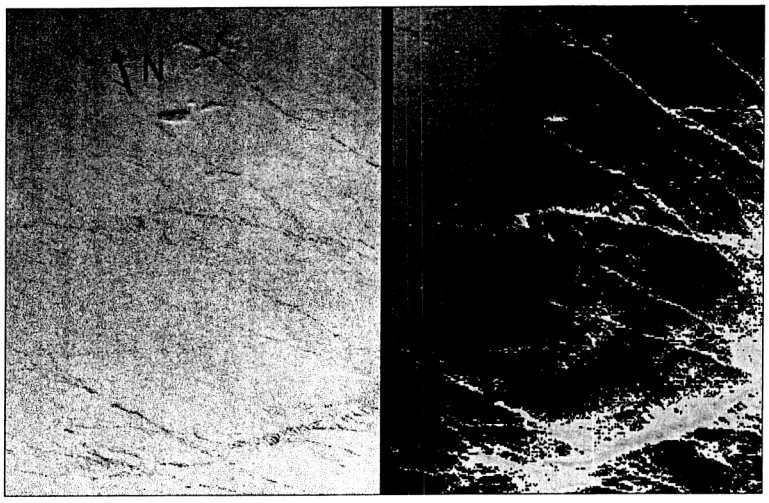

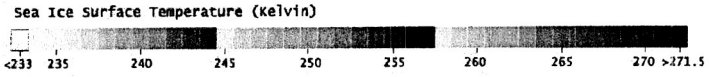

Figure 2

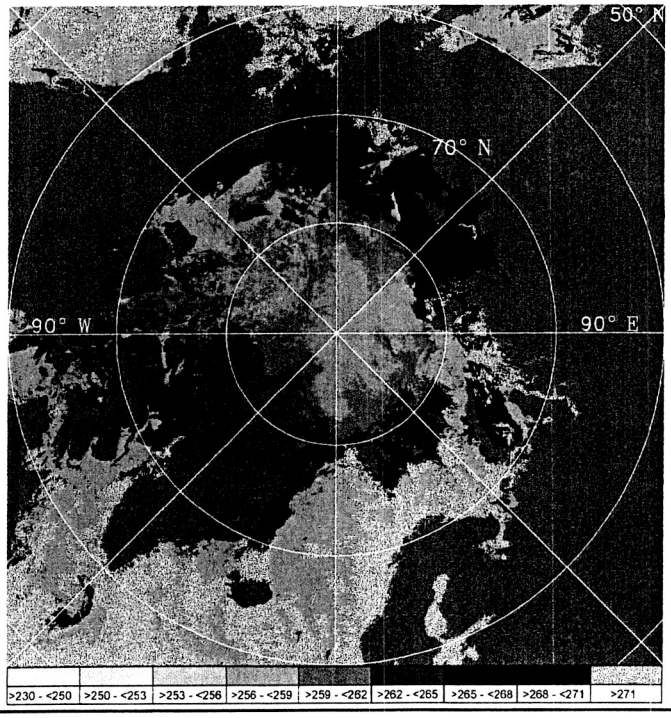

Figure 3a

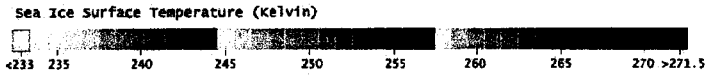

Figure 3b

Figure 4

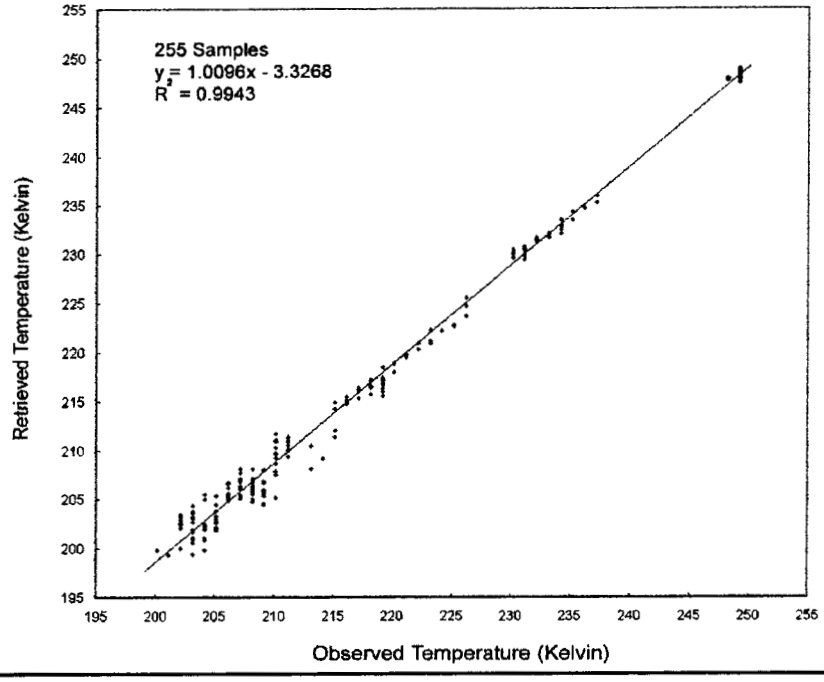

Figure 5